

Polyimide substrate-based polarization-dependent metamaterial absorber for terahertz applications

K. VIGNESHWARAN*, R. SAMSON DANIEL

Department of Electronics and Communication Engineering, K. Ramakrishnan College of Engineering, Samayapuram, Trichy, 621 112, India

A straightforward planar nonagon-shaped Terahertz (THz) Metamaterial Absorber (MMA) is devised and simulated for refractive index sensing applications. The proposed absorber employs three layers, with a polyimide dielectric substrate sandwiched between two copper layers, avoiding the need for multiple layers or numerous resonators in a single unit cell. The output absorption curves of this MMA exhibit polarization dependency, resonating at three frequencies in the x-direction and two frequencies in the y-direction, resulting in a total of five resonant frequencies across both directions. In the x-direction, the absorption rates at resonance frequencies of 0.78 THz, 0.793 THz, and 0.81 THz are 96.5%, 99.7%, and 99.8%, respectively. In the y-direction, the absorption rates are 99% for resonance frequencies of 0.791 THz and 0.799 THz. The refractive index (RI) sensing mechanism is analysed by placing a 1 μm analyte over the top patch structure, revealing a high quality factor and figure of merit (FOM) values of 371 and 47.6 RIU⁻¹, respectively. The physical mechanisms of the structure are investigated through electric field distribution, magnetic field distribution, and surface current distribution plots. Additionally, the polarization and incident angle characteristics of the structure are assessed by varying the angle values from zero degrees to ninety degrees. This absorber is intended for utilization in terahertz sensing applications.

(Received July 4, 2024; accepted February 3, 2025)

Keywords: Polarization dependent metamaterial absorber, Refractive index sensing, Terahertz

1. Introduction

Sensors are becoming increasingly vital across various industries, including scientific research, healthcare, food service, environmental monitoring, tracking systems, and soft robotics. These sensors enhance system [1] functionality by collecting data and providing feedback. In the realm of biosensors, this technology significantly improves human health by detecting biological signals and converting them into electrical outputs through appropriate signal conditioning circuitry. According to the World Health Organization (WHO), cancer is a severe disease that can affect any part of the body [2], often spreading and resulting in fatalities. However, early detection of cancer can potentially reduce mortality rates.

Different techniques can be utilized to detect biological signals. Electrochemical sensors, for instance, use methods such as potentiometry, voltammetry, impedimetry, and amperometry. Biosensors also come in other types, including thermoelectric, piezoelectric, optical, and various physical forms [3]. Each technique offers distinct advantages and disadvantages in terms of cost, sensitivity, and structure. Surface plasmon resonance (SPR) has become popular in optical methods due to its high precision, label-free detection, and minimal sample volume requirements [4]. This technique operates by sensing changes in the refractive index of an analyte. When light interacts with conducting electrons in metals or nanostructures [5], these changes alter the light's transmission, reflection, and absorption characteristics, causing a resonance shift that enables detection. These materials are synthetic periodic structures with wavelengths

shorter than that of the incident radiation. They possess a unique property known as a negative refractive index, which is not found in natural materials. The operational frequency of metamaterials is determined by their shape and material characteristics [6].

Metamaterials are used in many different applications, such as soft industrial automation sensors, coding schemes, electron microscopy, and detectors. Due to its special qualities, including non-ionization, the capacity to permeate a wide range of plastic materials, and the ability to identify biological fingerprints, the terahertz (THz) spectrum (0.1 to 10 THz) has attracted a lot of scientific interest [7] during the past 20 years. High-power THz sources and detectors have been developed as a result of developments in large optoelectronic devices, such as HEMT [8] structures and particle physics cascade lasers. Several investigations into motion sensors and sophisticated sources of electromagnetic energy have led to the development of different parts. Numerous THz metamaterial variations for a range of applications have been produced by research. Polarization-sensitive structures have received less attention from researchers than polarization-insensitive THz metamaterials [9-10].

To build a polarization-controlled metamaterial, two distinct strips of metallic conducting material were employed in a vertical and horizontal orientation. Through patch size variation, circularly polarized light absorption characteristics were obtained. A double absorption behaviour is also displayed by the framework [11]. For two distinct directions, an MMA that is dependent on polarization is conceived and constructed [12]. For varying polarization of the incident light, the frequency selective

MMA is resonated at single, dual, and triple band [13]. Polarization-dependent applications are the target market for THz MMA based on liquid crystals [14]. Graphene metal is used in the creation of tuneable polarization dependent MMA. In the creation of materials, the polymeric copolymer is used as a substrate material because of its low loss at the THz range. A bridge aperture, functionally graded outer edge filter was designed and tested effectively. This structure has polarization selectivity and perspective transmission properties for altering applications. The substrate's initiation has produced focused mode resonances in addition to the fundamental resonance [15]. Refractive index, temperature, pressure, and other sensing applications are also incorporated with MMAs.

Biosensing applications make use of the properties of the structure. By changing the refractive indices, the operating frequency range is altered. Biomedical signals were recognized with the use of this technique. The features of the sensor are determined by metrics including the value of merit, specificity, and factor (Q-factor) [16]. The number of papers in the Scopus dataset increased, suggesting that the researcher was more interested in terahertz MMs. A higher-quality factor value is used to assess the dual band MMA's sensing properties. A novel refractive index sensor and split-ring metamaterial absorber with a quad-band fan form has been developed. The graphene ring resonators that comprise each unit cell are split-ring and fan-shaped. Altering the DC-bias voltage of the absorber can modify its absorption spectrum [17]. Six-band terahertz metamaterial absorbers (MMAs) [18] are designed for temperature sensing applications using an InSb dielectric layer. Electromagnetic MMA-based pressure sensors [19] are created using inkjet and 3D modelling techniques. Four distinct THz MMA designs, which resonate at four different frequencies [20], are developed using a split relief design and an analyte thickness of three micrometres. For gas sensing applications, THz MMAs are constructed with a swastika-shaped structure using gold and GaAs materials. These designs and analyses demonstrate the need for polarization-sensitive sensors with high quality factors (High-Q) and figures of merit (FOM)[21].

The goal of this study is to develop and analyse a polarization-sensitive terahertz pentaband metamaterial. The sensor is designed to resonate at five distinct frequencies, enabling the detection of various analytes, each with unique patterns. The sensor's performance is evaluated by varying the refractive indices, which enhances the quality factor (Q), sensitivity, and figure of merit (FOM) values. This is accomplished without the need for multiple layers or numerous resonators within a single unit cell. The absorption curves of the designed metamaterial absorber (MMA) are polarization-dependent, resonating at three frequencies in the x-direction and two frequencies in the y-

direction. The refractive index (RI) sensing mechanism is assessed by placing a 1 μm analyte over the top patch structure.

The six-band terahertz metamaterial absorber (MMA), equipped with an InSb dielectric layer, is tailored for temperature monitoring applications. Additionally, a 3D and inkjet-based electromagnetic pressure sensor utilizing metamaterials is devised. Four distinct designs of terahertz MMAs, resonating at four different frequencies, are developed using split relief design techniques with an average thickness of three micrometres. Furthermore, a THz MMA design incorporating gold and GaAs materials, featuring a swastika-shaped structure, is crafted for gas sensing applications. These various designs and analyses underscore the necessity for investigating polarization-sensitive sensors endowed with High-Q and FOM characteristics.

2. Design and materials

The design and numerical analysis of the structure is studied by using CST Microwave Studio Software. The 3D view and front view of the proposed MMA based sensor structure is shown in Fig. 1. This absorber has only three layers. The substrate is sandwiched between the bottom metal plane and top patch structure. The metal used here is copper and substrate used here is polyimide with the dielectric constant of 3.5 and electric loss tangent of ($\tan \delta$) 0.0027. The conductivity of the metal is 5.8×10^7 S/m [22]. The parameters and values used to design the MMA is shown in Table 1.

Ground plane and substrate having the same length and width of 0.5 mm. Top patch structure consists of nonagon shaped resonator. Its outer radius is 0.24 mm and inner radius is 0.16 mm. The proposed absorber design is a planar structure and it's having only three layers and easy top patch material design.

Table 1. Geometrical values of designed MMA

Parameters	Values (mm)
Length and width of the ground plane	(0.5×0.5)
Length and width of the substrate	(0.5×0.5)
Outer Radius (R2)	0.24
Inner Radius (R1)	0.16
Thickness of the patch	0.001
Thickness of the substrate	0.125

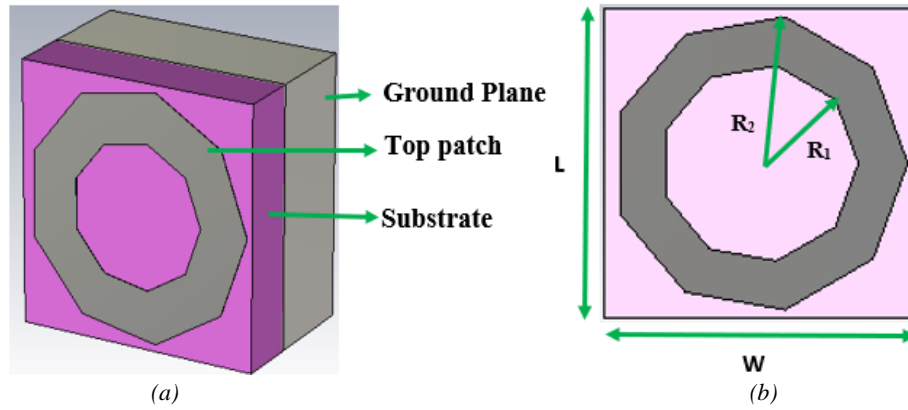


Fig. 1. Perspective view and front view of proposed MMA (colour online)

3. Boundary conditions and absorption rate

The boundaries are defined at three coordinates namely x , y and z . The unit cell boundary condition is applied at the x and y directions and open (add space) boundary condition is applied at the z direction. Defined Boundaries with axis are shown in Fig. 2.

Generally, the absorption rate of the absorber structure is calculated by using the reflection (RE), transmission (TR) and angular frequency (ω) values. $AB(\omega) = 1 - RE(\omega) - TR(\omega)$, this formula is used to calculate the absorption rate of the absorber. If the thickness of the bottom plane is larger than the skin depth transmission value is zero. By matching the impedance condition makes reflection value as zero. So, it will make a way to get higher absorptivity.

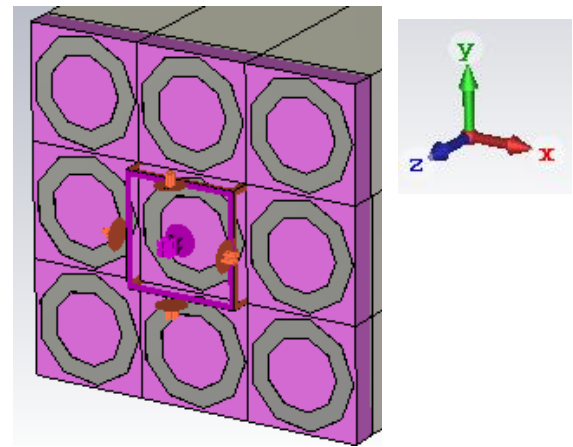


Fig. 2. Boundary conditions of terahertz MMA (colour online)

4. Results and discussions

4.1. Absorption characteristics

The finite element method-based CST Microwave Studio is used to design and simulate the proposed structure. The absorption curves are showing the absorption rate of the MMA for both Transverse Electric (TE) and Transverse Magnetic (TM) modes which, is shown in Fig. 3. At the TE mode the absorber is resonated at three different frequencies at 0.78 THz, 0.793 THz and 0.81 THz with the absorption rate of 96.5 %, 99.7 % and 99.8 % And in the TM mode the absorption rate is 99 % and 99 % at the resonant frequency of 0.791 THz and 0.799 THz. Above 95 % of absorption rate is achieved at all five different frequencies with simple structure. Resonant frequency and corresponding absorption rate values are tabulated in Table 2.

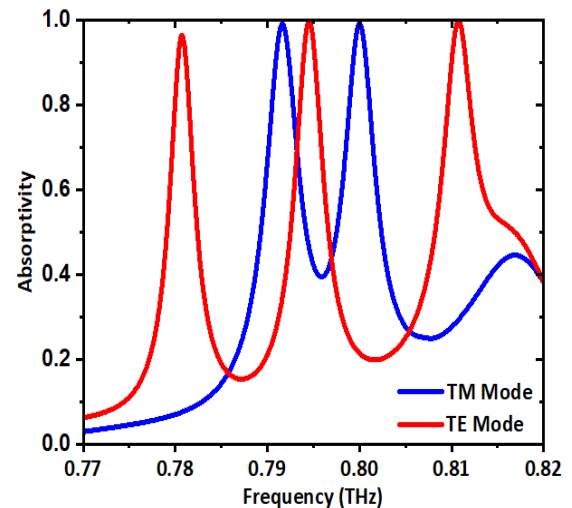


Fig. 3. Absorption rate of the proposed MMA (colour online)

Table 2. Frequency and absorption rate values of designed MMA in TE and TM modes

Mode	Frequency (THz)	Absorptivity (%)	No. of bands
TE Mode	0.78, 0.793, 0.81	99.8, 99.7, 96.6	3
TM Mode	0.791, 0.799	99, 99	2

4.2. Polarization and angular stability

The polarization angle and oblique incident angle behaviour of the structure is analysed from changing the angle values. In this case we have changed the angle values from zero degree to ninety degree which is shown in Fig. 4. For all the angles of operation resonant

frequency and absorption rate is did not vary so it is polarization angle (ϕ) and oblique incident angle (θ) insensitive in nature.

4.3. Surface plasmonic study

The plasmonic behaviour of the surface is analysed from electric field, magnetic field and surface current distribution plots. This plot explained current distribution over the patch and substrate layer. The electric field distribution of the structure is shown in Fig. 5. Fig. a, b, c represents the e-field distribution at 0.78 THz, 0.793 THz and 0.81 THz frequencies. And figure c, d represents the e-field distribution at 0.791 THz and 0.7939 THz frequencies. For all the five resonant frequencies the electric field distribution is maximum at whole patch structure and surface of the dielectric layer.

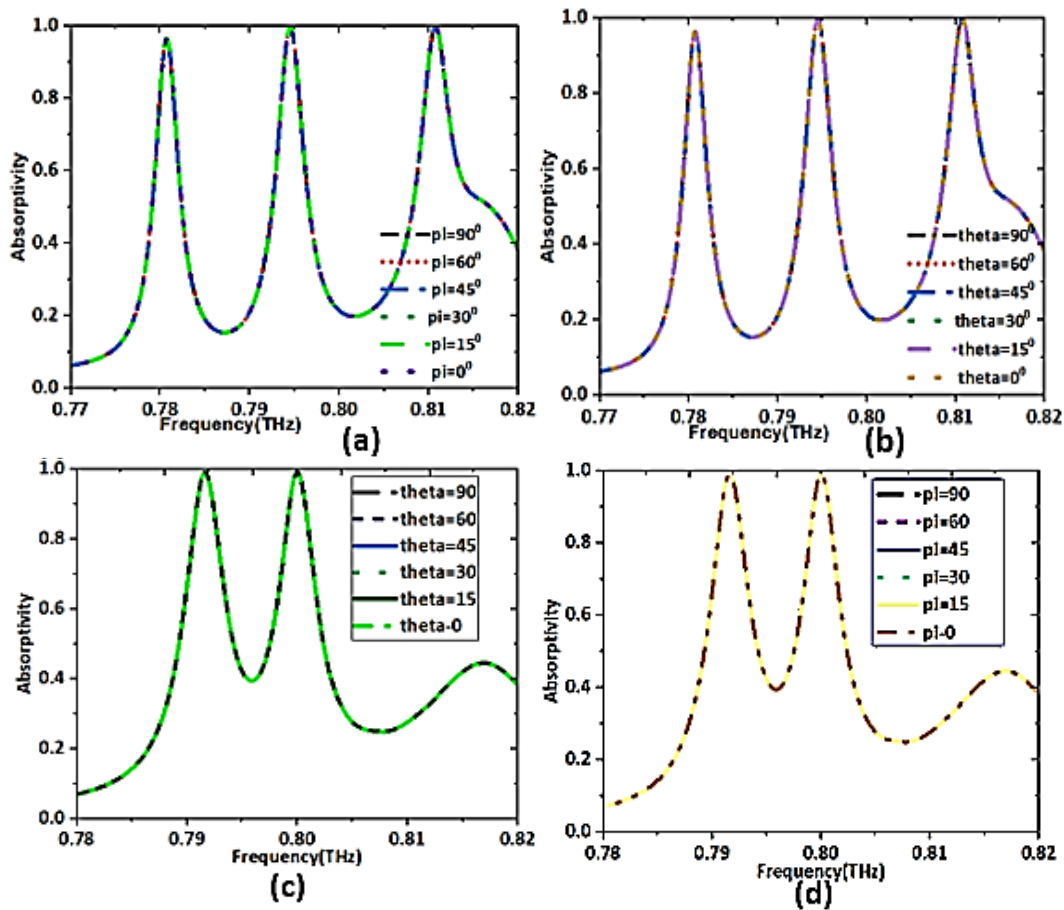


Fig. 4. Polarization (ϕ) and Incident Angle (θ) Stability for (a) (b) X direction (c) (d) Y direction (colour online)

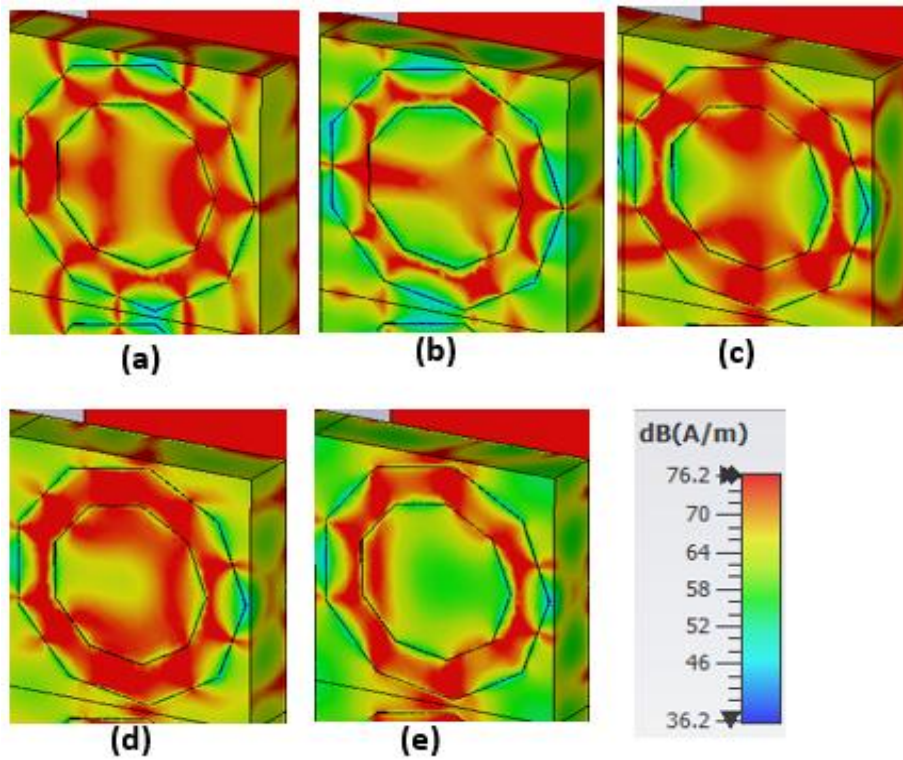


Fig. 5. [a-c] Electric field distribution in x direction (a) 0.78 THz, (b) 0.793 THz, (c) 0.81 THz, [d-e] Electric field distribution in y direction (d) 0.791 THz, (e) 0.799 THz (colour online)

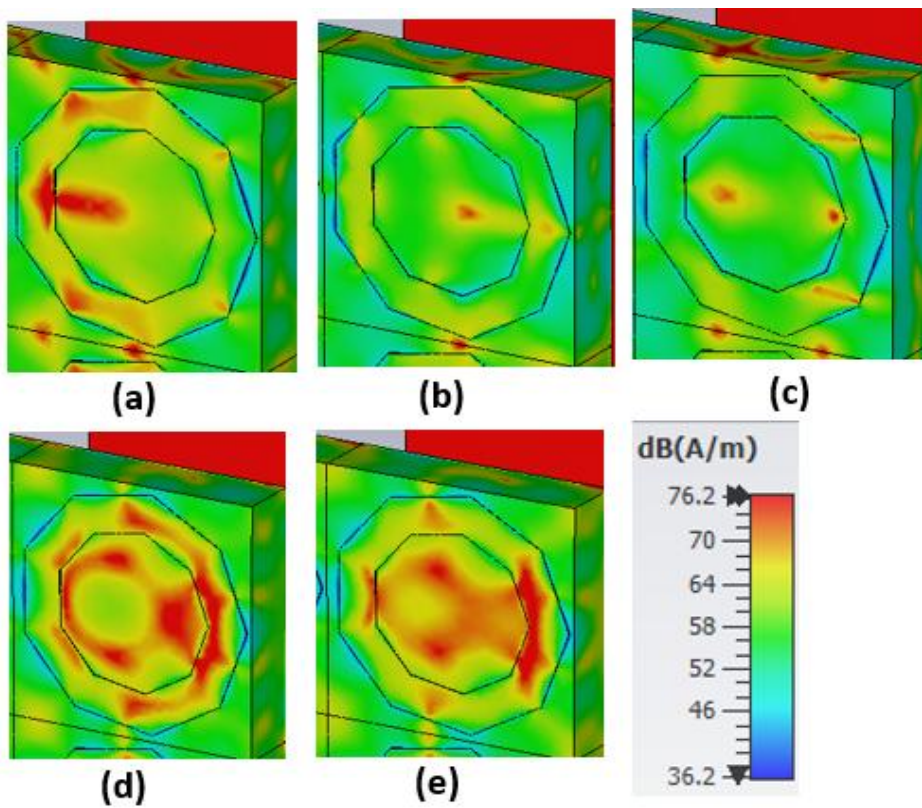


Fig. 6. (a-c) Magnetic field distribution in x direction (a) 0.78 THz, (b) 0.793 THz, (c) 0.81 THz, (d-e) Magnetic field distribution in y direction (d) 0.791 THz, (e) 0.799 THz (colour online)

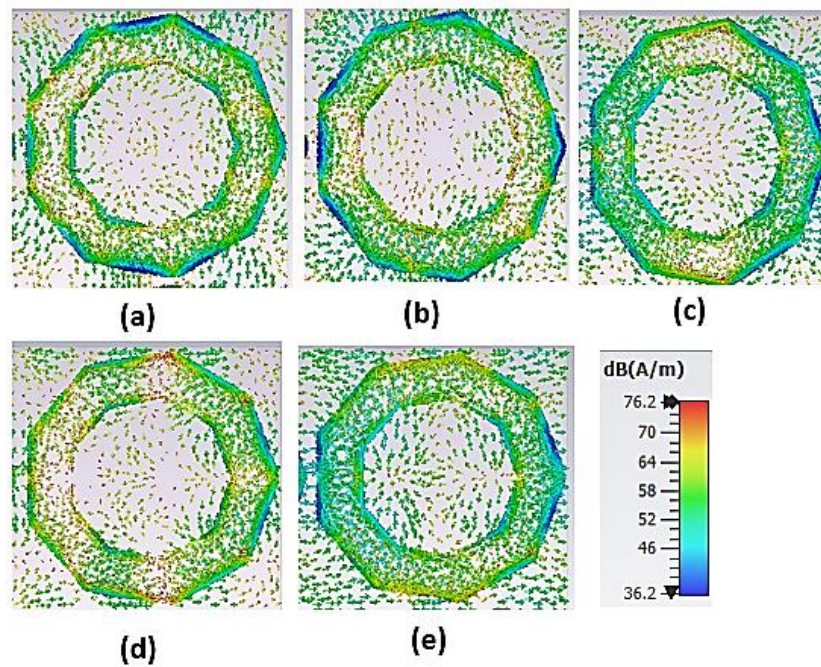


Fig. 7. [a-c] Surface current distribution in x direction (a) 0.78 THz, (b) 0.793 THz, (c) 0.81 THz, [d-e] Surface current distribution in y direction (d) 0.791 THz, (e) 0.799 THz (colour online)

The magnetic field distribution of the structure is shown in Fig. 6. Fig. 6 (a, b, c) represents the m -field distribution at 0.78 THz, 0.793 THz and 0.81 THz frequencies. And Fig. 6 (d, e) represents the m -field distribution at 0.791 THz and 0.7939 THz frequencies. For all the five resonant frequencies the electric field distribution is maximum at some places of the patch structure and surface of the dielectric layer.

The surface current distribution plot of the MMA structure is shown in Fig. 7. Fig. 7 (a, b, c) represents the surface current distribution at 0.78 THz, 0.793 THz and 0.81 THz frequencies. And Fig. 7 (d, e) represents the surface current distribution at 0.791 THz and 0.7939 THz frequencies. For all the five resonant frequencies the surface current distribution is maximum at whole patch structure and some places of surface of the dielectric layer.

4.4. Parametric study

The study of parameters while designing the MMA gives the chance to choose a best absorption rate value. In this case top patch having nonagon shaped resonator. The outer and inner radius of the nonagon is 0.24 mm and 0.16 mm. The inner radius value is changed from 0.12 mm to 0.22 mm with the step size of 0.2 mm. When the inner radius is 0.16 mm the absorber resonated at three different frequencies with maximum absorption rate compare to other radius values. Fig. 8 shows the absorption rate for different frequencies while changing the inner radius value.

5. Sensing mechanism

Sensing capability of the structure is studied from placing 1 μ m or 0.001 mm analyte over the top patch layer which is shown in Fig. 9. The resonant frequency is shifted while

placing the analyte over the top patch layer. From this frequency shift the sensing nature of the structure is studied.

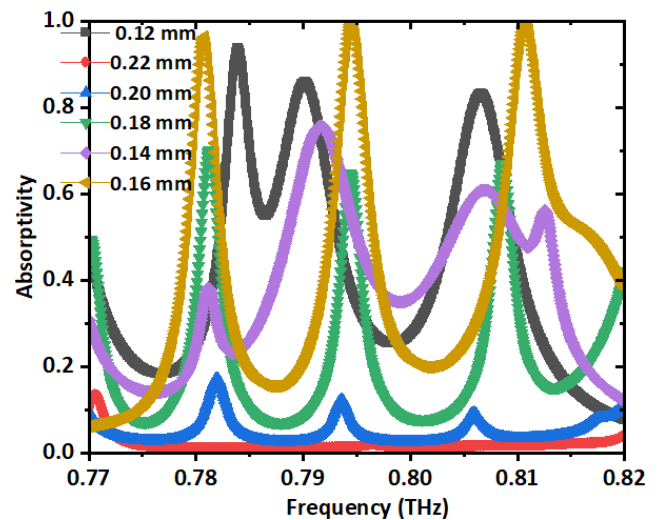


Fig. 8. Absorption curves for different values of inner radius (RI) (colour online)

The RI of regular and affected cells will change, as in the case of cancer, DNA and RNA studies [23-24]. For these applications, a RI sensor is used. All over the analysis, the analyte thickness is held constant at 1 μ m. The reason for this is to comprehend the sensor's applicability in detecting the lower limit value. The shift in resonances is insignificant for analyte thicknesses less than 0.5 μ m [25-27]. As a result, the minutest thickness is reserved at 1 μ m. There are some parameters needed to analyse the sensing which are Quality factor (Q), Full Width Half Maximum (FWHM), Figure of Merit (FOM) and Sensitivity (S). If the

Quality factor is high the structure will be used in sensing applications. In this study, the sensing is analysed for both TE and TM mode. Fig. 10 (a) and (b) shows the absorption curves after placed the analyte over the top patch layer for TE and TM modes. The frequency is shifted from original position to the lower frequency side while changing the refractive index (n) values from 1 to 1.8. The original frequency, shifted frequency, FWHM, Q , Sensitivity and FOM values are shown in Table 3 for TE mode. The original frequencies are 0.78 THz, 0.793 THz and 0.81 THz. After analyte layer the frequency is shifted into 0.76 THz, 0.78 THz and 0.80 THz respectively.

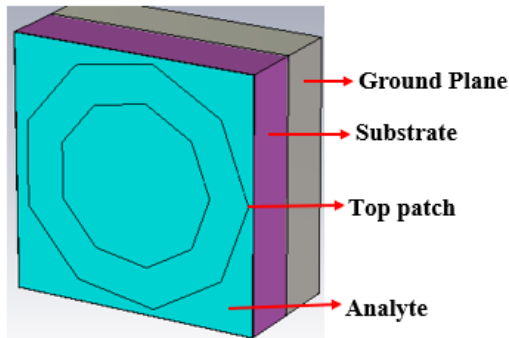


Fig. 9. Analyte structure placed above the substrate layer (colour online)

At frequency 0.76 THz the Q factor is high compare to other frequencies. So, the sensitivity and FOM of the first frequency is also high which values are tabulated in Table 3.

6. Conclusion

The proposed planar structure's sensing ability is assessed by changing the over layer refractive index (RI) from 1 to 1.8. The RI of regular and affected cells will change, as in the case of cancer, DNA and RNA studies. For these applications, a RI sensor is used. All over the analysis, the analyte thickness is held constant at 1 μm . The reason for this is to comprehend the sensor's applicability in detecting the lower limit value. The shift in resonances is insignificant for analyte thicknesses less than 0.5 μm . As a result, the minutest thickness is reserved at 1 μm . From the RI sensing analysis this MMA based sensor produces high quality factor and FOM value of 371 and 47.6 RIU^{-1} respectively. And the output absorption curves for this designed MMA are polarization dependent because it resonated at three frequencies at the x-direction and in the y-direction it is resonated at two different frequencies. In the x and y direction it is resonated at five different frequencies so it is polarization dependent. The physical mechanism of the structure is studied from electric field distribution, magnetic field distribution and surface current distribution plots. Polarization and incident angle characteristics of the structure is analysed by varying the angle values from zero degree to ninety degree. This absorber will be used in terahertz sensing and polarization imaging applications.

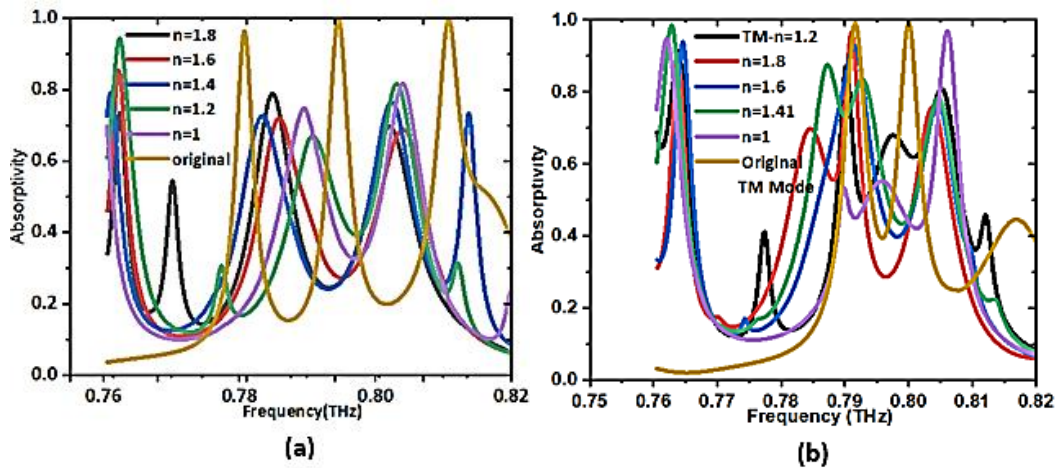


Fig. 10. Frequency shifting responses for (a) TE Mode (b) TM Mode (colour online)

Table 3. Sensitivity, FOM, FWHM and Q values of proposed MMA

(f1) (THz)	A (%)	(f2) (THz)	df=f1-f2	FWHM	Q=f/FWHM	S=df/dn (GHz)	FOM=S/FWHM (RIU^{-1})
0.78	96.5	0.76	0.02	2.1	371	100	47.6
0.79	99.7	0.78	0.01	2.4	330	50	20.83
0.81	99.8	0.80	0.01	2.35	352	50	21.27

FOM-Figure of Merit, FWHM-Full Width Half Maximum, S-Sensitivity, Q-q factor, df-frequency difference, f1-Original Frequency, f2- Shifted Frequency

References

- [1] M. Silveirinha, N. Engheta, *Phys. Rev. Lett.* **97**, 157403 (2006).
- [2] S. Banerjee, P. Dutta, A. V. Jha, B. Appasani, M. S. Khan, *IEEE Sensors Lett.* **6**, 1 (2022).
- [3] M. Coroş, S. Pruneanu, R. I. Stefan-van Staden, *J. Electrochem. Soc.* **167**, 037528 (2020).
- [4] S. Sen, M. Abdullah-Al-Shafi, M. A. Kabir, *Sensing and Bio-Sensing Research* **30**, 10037 (2020).
- [5] S. A. Taya, *J. Mater. Sci. Mater. Electron.* **32**(24), 28406 (2021).
- [6] Shuhong Li, Platte Amstutz, Cha-Mei Tang, Jun Hang, Peixuan Zhu, Yunqi Zhang, Daniel R. Shelton, Jeffrey S. Karns, *Methods in Molecular Biology* **503**(3), 389 (2009)
- [7] Sunil Jorwal, Ashish Dubey, Rajeev Gupta, Smriti Agarwal, *Sensors and Actuators A: Physical* **354**, 114283 (2023).
- [8] X. Huang, W. Ye, J. Ran, Z. Zhou, R. Li, B. Gao, *IEEE Sensors Journal* **23**, 3573 (2023).
- [9] Neha Niharika, Sangeeta Singh, Pankaj Kumar, *Photonics and Nanostructures - Fundamentals and Applications* **54**, 101116 (2023).
- [10] Ben-Xin Wang, Yuanhao He, Nianxi Xu, Xiaoyi Wang, Yanchao Wang, Jianjun Cao, *Results in Physics* **17**, 103077 (2020).
- [11] Fangrong Hu, Taobo Zou, Baogang Quan, Xinlong Xu, Shuhui Bo, Tao Chen, Li Wang, Changzhi Gu, Junjie Li, *Optics Communications* **332**, 321 (2014).
- [12] Guangsheng Deng, Tianyu Xia, Yong Fang, Jun Yang, Zhiping Yin, *Applied Sciences* **7**, 580 (2017).
- [13] Guangsheng Deng, Yujiao Lu, Zhiping Yin, Weien Lai, Hongbo Lu, Jun Yang, Aifeng Yang, Yang Ye, Dayong Liu, Baihong Chi, *Electronics* **7**(3), 27 (2018).
- [14] A. Ferraro, D. C. Zografopoulos, R. Caputo, R. Beccherelli, *Applied Physics Letters* **110**, 141107 (2017).
- [15] L. N. Deekonda, S. K. Sahu, A. K. Panda, *Lecture Notes in Electrical Engineering*, Springer, Singapore, 987 (2023).
- [16] Bhargav Appasani, Avireni Srinivasulu, Cristian Ravariu, *Defence Technology* **22**, 69 (2023).
- [17] Haijun Zou, Yongzhi Cheng, *Optical Materials* **88**, 674 (2019).
- [18] Heijun Jeong, Yepu Cui, Manos M. Tentzeris, Sungjoon Lim, *Additive Manufacturing* **35**, 101405 (2020).
- [19] H. Sudarsan, K. Mahendran, S. Rathika, *International Journal of Communication Systems*, Wiley, 34 (2024).
- [20] S. Banerjee, Purba Dutta, Snehashish Basu, Sunil Kumar Mishra, Bhargav Appasani, Sarita Nanda, Yadgar I. Abdulkarim, Fahmi F. Muhammadsharif, Jian Dong, Amitkumar V. Jha, Nicu Bizon, Phatiphat Thounthong, *Symmetry* **15**(1), 24 (2023).
- [21] Z. Liu, L. Wang, M. Hua, X. Liu, F. Qian, G. Xie, Y. Ning, Y. Shi, X. Wang, F. Yang, *AIP Advances* **10**(7), 075014 (2020).
- [22] Sachin Kalraiya, Raghvendra Kumar Chaudhary, Ravi Kumar Gangwar, *AEU - International Journal of Electronics and Communications* **135**, 153752 (2021).
- [23] E. Manikandan, K. A. Karthigeyan, A. Arivarasi, E. Papanasam, *IEEE Photonics Journal* **15**, 1 (2023).
- [24] Xunjun He, Shaopeng Li, Xingyu Yang, Shuang Shi, Fengmin Wu, Jiuxing Jiang, *Journal of Electromagnetic Waves and Applications* **31**(1), 91 (2017).
- [25] K. Mahendran, H. Sudarsan, S. Rathika, *AEU - International Journal of Electronics and Communications* **161**, 154543 (2023).
- [26] K. Mahendran, Sathish Kumar Danasegaran, R. Indhu, S. Annie Angeline Preethi, *Journal of Optoelectronics and Advanced Materials* **26**(3-4), 106 (2024).
- [27] H. Sudarsan, K. Mahendran, S. Rathika, *Results in Optics* **15**, 100653 (2024).

*Corresponding author: vigneshwaran.krce@gmail.com